Journal of
Mechanics of
Materials and Structures

# OBSERVATIONS OF ANISOTROPY EVOLUTION AND IDENTIFICATION OF PLASTIC SPIN PARAMETERS BY UNIAXIAL TENSILE TESTS

Yangwook Choi, Mark E. Walter, June K. Lee
and Chung-Souk Han

Volume 1, Nº 2 February 2006

mathematical sciences publishers

JOURNAL OF MECHANICS OF MATERIALS AND STRUCTURES
Vol. 1, No. 2, 2006

# OBSERVATIONS OF ANISOTROPY EVOLUTION AND IDENTIFICATION OF PLASTIC SPIN PARAMETERS BY UNIAXIAL TENSILE TESTS

YANGWOOK CHOI, MARK E. WALTER, JUNE K. LEE AND CHUNG-SOUK HAN

Micromechanical effects such as the development of crystallographic texture and of dislocation structures lead to evolution of material anisotropy during plastic deformation. The anisotropy of sheet metals is commonly quantified by its $R$-values. The $R$-value is defined as the ratio of the transverse strain to the thickness strain at a certain longitudinal strain, and it changes if the anisotropy changes. Conventional hardening models do not account for the evolution of anisotropy along an arbitrary orientation. Therefore, although $R$-values are measured from experiments, predictions of hardening behavior based on $R$-values using conventional hardening models do not reproduce the experiments for arbitrary orientation. The $R$-value evolution for large strains can be observed in simple uniaxial tension tests by measuring the transverse and longitudinal strains continuously up to large strains. A digital image correlation (DIC) method is introduced as superior to strain gages for measuring large strains. To model the experimental response, a rotational-isotropic-kinematic (RIK) hardening model is investigated. Because of this model's ability to represent the rotational evolution of the anisotropy, it can predict the hardening behavior for non-RD and non-TD directions. Methods to identify the plastic spin and kinematic hardening parameters are also discussed.

## 1. Introduction

In sheet metal forming and springback processes, incorporating evolution of material anisotropy is important in order to obtain accurate predictions. Cold rolled sheet metals are known to have initial anisotropy, incurred during the rolling process. The anisotropy causes different flow stresses with respect to the orientation that is measured from the rolling direction (RD). The different flow stresses have significant effects on the forming process: different earing of edges, punch force-displacements, and springback, etc. To address the material anisotropy, anisotropic yield functions such as those of [Hill 1948; 1990] and [Barlat et al. 1991; 1997; 2003] have been developed. Hill's quadratic yield function [Hill 1948] is known to

*Keywords:* Anisotropy evolution, $R$-value evolution, DIC measurements, rotational hardening.

be appropriate for BCC materials such as mild steel, while Barlat's yield function [Barlat et al. 1991; 1997; 2003] is good for FCC materials such as aluminum alloys. However, these yield functions do not account for the *evolution* of material anisotropy during the plastic deformation.

The evolution of anisotropy has been observed by both micromechanical and macromechanical experiments [Boehler and Koss 1991; Bunge and Nielsen 1997; Kim and Yin 1997; Peeters et al. 2001]. At a micromechanics level, the anisotropy evolution is generally considered to be the result of the crystallographic texture development, which changes the preferred orientation of grain aggregates, and the development of substructures [Peeters et al. 2001]. Using micromechanical approaches, the evolution of anisotropy has been observed and modeled by many investigators [Agnew and Weertman 1998; Asaro 1983; Beaudoin et al. 1994; Kocks et al. 1998; Nakamachi and Doug 1997]. On the other hand, the anisotropy evolution has been observed and modeled by using macromechanical approaches that rely on phenomenological descriptions [Boehler and Koss 1991; Kim and Yin 1997; Kuroda 1997; Dafalias 2000; Han et al. 2002].

For sheet metals, $R$-values in several directions are used to represent the planar anisotropy and to compare the anisotropy between different materials. The $R$-value is defined as the ratio of transverse strain to thickness strain at a certain longitudinal strain. Since $R$-values are different for different longitudinal strains, $R$-values are usually provided along with the longitudinal strain at which the transverse strains were measured.

Even though the $R$-values are used to define the anisotropic relationship of the hardening curve between a certain direction and the RD, the computed hardening curve may not properly predict the experiment results for orientations not in the RD or TD (transverse direction) when conventional hardening models are used. The computed hardening curves in three directions are compared with the experimental results in Figure 1. The computed curves were generated by ABAQUS/Standard using Hill's quadratic yield function and an isotropic hardening model. The material is deep drawing quality (DDQ) mild steel which is used for the NUMISHEET 2002 benchmark problem [Yang et al. 2002]. The curves of the RD and TD correlate quite well with the experimental results. However, the computed 45° orientation curve overestimates the experiment when constant $R$-values are used: $R_0 = 2.64$, $R_{45} = 1.57$, and $R_{90} = 2.17$.

The use of constant $R$-values is effective for characterizing the flow stresses in RD and TD. However, it is not capable of modeling the flow stress in the 45° orientation. It is assumed that the unexpected higher estimation of the hardening at 45° in Figure 1 can be explained by the evolution of anisotropy and the subsequent $R$-value evolution for the orientation. In addition, Hill's yield criterion [1948] has

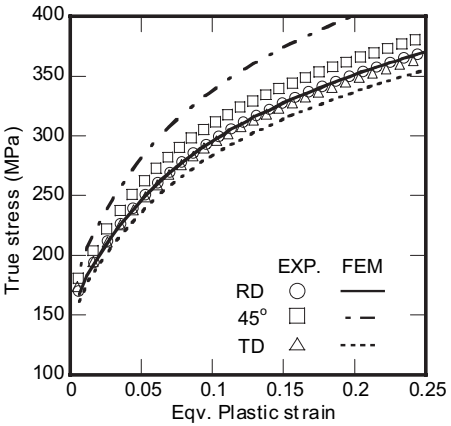


**Figure 1.** Flow stresses in three orientations, compared to measured data from NUMISHEET 2002 [Yang et al. 2002]. ABAQUS/Standard was used to compute the curves by using constant $R$-values. The flow stress at 45° overestimates the experiments, while the others correlate with experiments relatively well.

major drawbacks in predicting flow stress curves that depend on the loading orientation. In other words, the dependence of the yield stress on orientation is poorly predicted by the conventional theory [Banabic et al. 2000]. These shortcomings are usually interpreted to be the result of not incorporating the evolution of anisotropy during the plastic deformation.

Understanding the evolution of anisotropy is critical for predicting material behavior in large strain deformation. It is also essential to be able to represent the anisotropy evolution in multiaxial and multipath loading. To model the multiaxial and multipath elastoplastic deformation of planar anisotropic materials, an RIK (rotational-isotropic-kinematic) hardening model [Choi et al. 2006a] is proposed to incorporate rotation of the yield surface with the isotropic combined kinematic hardening model. To measure anisotropy evolution, tensile tests for RD, TD, and 45° orientations were performed.

A simple method to measure the rotation of the symmetry axes is suggested with the following assumptions: the anisotropy of the yield surface shape can be described by the rotation of the orthogonal symmetry axes, and the symmetry axes will not rotate if the loading is along the symmetry axes. The method requires tensile experiments with continuous measurement of $R$-values for specimens cut at 45° to the RD. According to the theory, the symmetry axes do not rotate for the deformation along the RD or TD. To measure the strains continuously up to large strains, we used the DIC (digital image correlation) method developed by

Sutton et al. [1983]. DIC is a technique that compares digital images of a specimen surface before and after deformation to deduce its two-dimensional surface displacement field and strains; see, for example, [Vendroux and Knauss 1998]. In spite of its low accuracy at small strains, DIC can be used at large strains and is simple to implement. Although large strains were measured using digital images of grid marks on uniaxial sheet metal specimens by Rao and Mohan [2001], the grid deformation was not used to determine $R$-values. The authors are not aware of any other investigations that use the DIC method to determine $R$-values.

Here we present a DIC-based experimental method for determining anisotropy evolution and demonstrates how the material parameters for the RIK hardening model can be determined from the simple tensile experiments.

## 2. Definition of the $R$-value

The definition of the $R$-value for a planar anisotropic material is the ratio of transverse strain ($\varepsilon_w$) to thickness strain ($\varepsilon_t$) and is therefore given by Hill [1950] as

$$R = \frac{\varepsilon_w}{\varepsilon_t}. \tag{1}$$

Because the specimen thickness is generally small compared to the other dimensions, an accurate measurement of the strain in the thickness direction for sheet metals is difficult. By applying the constant volume condition for plastic deformation, Equation (1) can be reformulated using the longitudinal strain ($\varepsilon_l$) as

$$R = \frac{\varepsilon_w}{\varepsilon_t} = -\frac{\varepsilon_w/\varepsilon_l}{(1+\varepsilon_w/\varepsilon_l)},$$

which is widely used to measure $R$-values. With these formulas the $R$-values are determined by fitting the slope ($\varepsilon_w/\varepsilon_l$) of the $\varepsilon_w - \varepsilon_l$ (transverse strain versus longitudinal strain) curve of experiments. An example for DDQ material used in NUMISHEET 2002 benchmark problem [Yang et al. 2002] is shown in Figure 2 (left). For DDQ, the TD and RD lines are very relatively straight. It should be noted that although the 45° response appears to be linear, it has measurable nonlinearity. Given the linear and nonlinear responses, the anisotropy in the RD and TD expressed through $R$-values remains constant, as seen in Figure 2 (right), while the $R$-value evolves for tensile tests in the 45° orientation.

This is consistent with the assumptions stated in the introduction that no rotation of the anisotropy axes will occur for the loading along the RD or TD. As shown in Figure 3, Stout and Kocks have obtained similar $R$-value evolution on a cube of copper with rolling texture [Kocks et al. 1998].

It is evident that $R_{45}$ evolves with the strain. However, the current industry practice is to measure an $R$-value at a certain longitudinal strain (15–20%) and

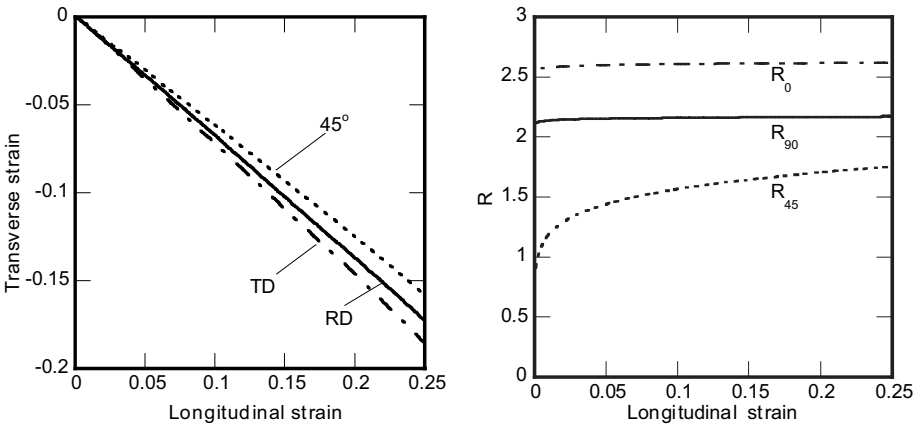


**Figure 2.** Transverse strain versus longitudinal strain of DDQ (left). Fitted $R$-values for each orientation (right). The $R_{45}$ value is evolving with the strain and documents the evolution of anisotropy in the 45° orientation.

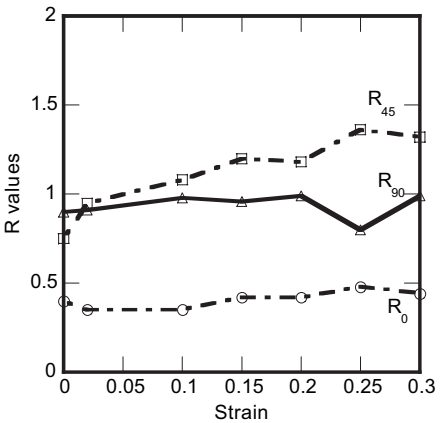


**Figure 3.** $R$-value measurements for rolled copper in compression experiments. Particularly $R_{45}$ shows significant changes. >From [Kocks et al. 1998].

use it as a constant. A suitable modeling method for the anisotropy evolution is addressed by Choi et al. [2006a].

## 3. Experimental setup

Experiments were performed on an MTS Model 810 servohydraulic load frame with an Instron 8500 digital controller. Figure 4 shows the experimental setup. The controller was operated in displacement control mode. Load was measured

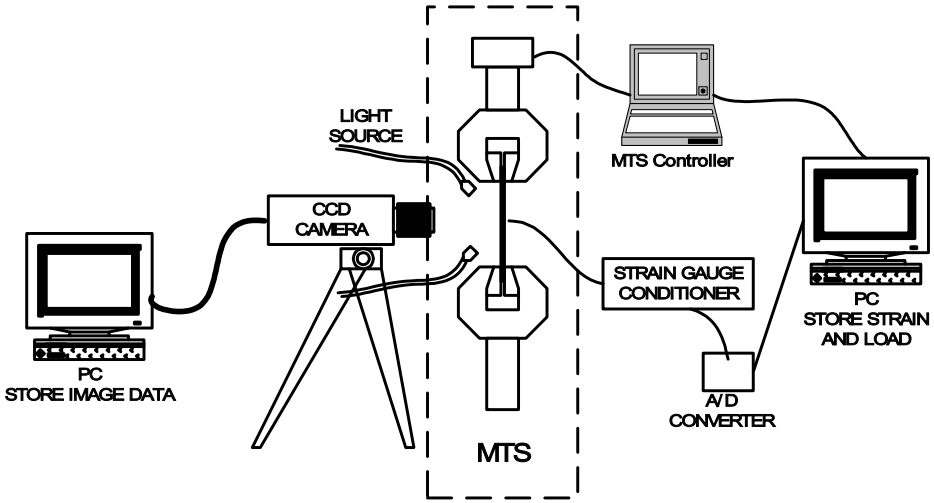


**Figure 4.** Schematic diagram of the experimental setup.

from a 25 MT load cell and was subsequently converted to true stress. For some experiments, strain gages were used to verify the accuracy of the DIC strain measurement.

Large strains were measured using DIC, the required images being acquired by a Pulnix TMC-9701 digital CCD camera with a resolution of $768 \times 472$ pixels at a continuous rate of 4 frames per second. To minimize intensity change during the experiment, a Schott KL1500 directed light source was used to illuminate the specimen.

Specimens used in the experiments were cut from sheet metal at 0°, 45°, and 90° to the RD direction. Specimens were 1 inch wide and 0.039 inch (1 mm) thick. Since the view of the CCD camera is fixed and only the lower grip of the load frame moves, the region of interest has significant downward displacement. Therefore, the size of the specimen must be carefully chosen to ensure that a significant portion of the originally undeformed image remains inside the camera's view for all subsequent deformation. For this reason, 1.5 inch gage length specimens were used. FEM simulations were performed to confirm that the region where strains were measured was far enough away from the grips to avoid grip effects. The results of these FEM simulations are shown in Figure 5(a). By comparing transverse strain versus longitudinal strain curves for four locations along the specimen centerline — see Figure 5(a) — no significant differences were observed in the curves shown in Figure 5(b). Hence, end effects do not influence the region of interest.

The DIC method works best when the starting image contains a random pattern that can carry the specimen deformation exactly. To create such a random pattern

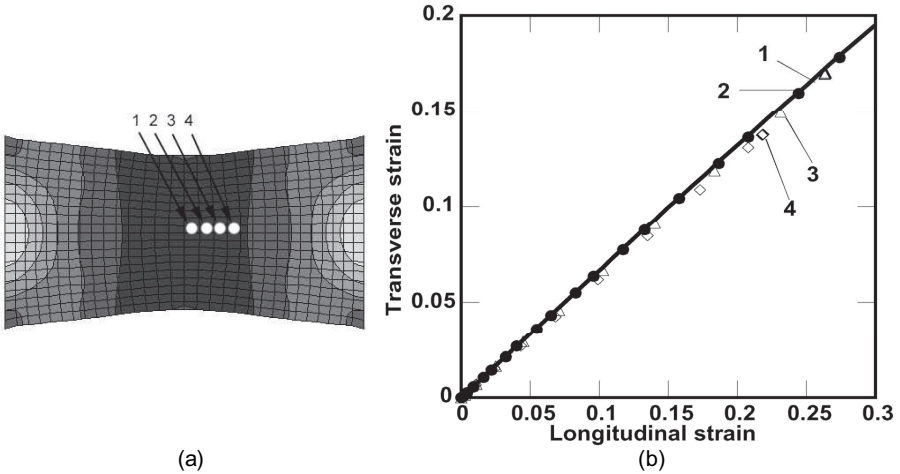


**Figure 5.** FEM validation of specimen dimensions to avoid grip effects: (a) strain measurement locations; (b) computed strains.

on the current specimens, spray paint was used. First white paint provided a bright background and then black spray paint gave a high contrast speckle pattern. The black paint was applied by spraying parallel to the specimen surface and letting paint droplets fall randomly on the specimen. Examples of the random pattern before and after deformation are shown in Figure 6.

The DIC program was set to measure incremental transverse and longitudinal strain between subsequent images. For random patterns such as the one shown in Figure 6, the best subset size was $100 \times 100$ pixels, corresponding to $4.2 \times 4.2$ mm.

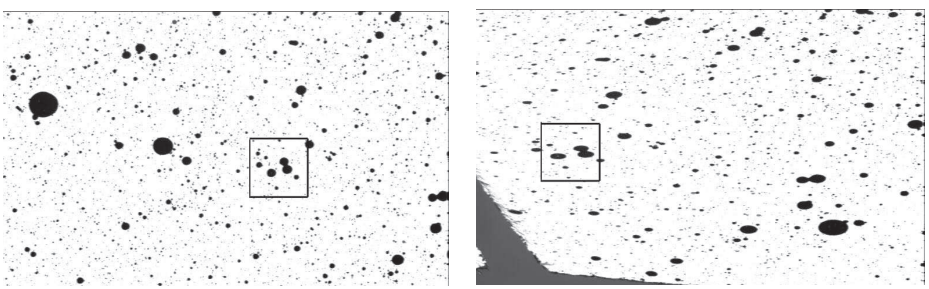


**Figure 6.** The random pattern sprayed on the specimen and captured by the CCD camera (a) before and (b) after deformation. The small rectangles highlight a $100 \times 100$ pixel subset of the image that has been deformed.

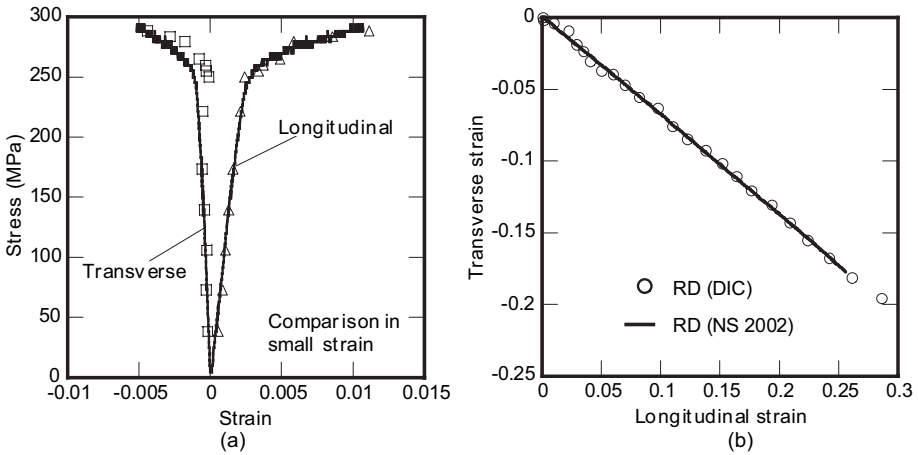


**Figure 7.** (a) Comparison of stress-strain measurement by DIC (symbols) and strain gauge (lines) for tensile test on RD specimens; (b) comparison of strain measurement by DIC and NUMISHEET 2002 data.

The displacement was measured at 25 equally spaced points in the subset. Since the subset used for correlation at the beginning of the loading has undergone significant translation by the end the deformation, it was necessary to devise an algorithm to track the approximate position of each subset used for correlation. Total strain was obtained by adding the incremental strains. In order to reduce measurement error, the correlation was performed on all 25 points in the subset, and then strain values that were beyond one standard deviation were eliminated. The average strain was then determined from the remaining strain values. The original DIC program was written in FORTRAN and C by Vendroux and Knauss [1998]. The modifications to track the overall displacement of the subsets and to treat the strain measurements statistically were done by the authors. The accuracy of the DIC method for strain measurements is demonstrated by comparison with a strain gage for smaller strains and with the data provided by NUMISHEET 2002 [Yang et al. 2002] for larger strains. The results are shown in Figure 7. The strain measurement with DIC has poor resolution at lower strains but shows quite good correlation with the NUMISHEET 2002 data at higher strains. Usually it is difficult to measure large strains with a strain gage, but DIC can measure 25–30% strains with relative ease. The limitation at strains greater than 30% is related to the loss of adherence of the applied speckle pattern to the specimen surface.

## 4. Hardening model

The procedure for modeling isotropic, kinematic and rotational hardening is rather complex. Since this article is mainly concerned with experimental findings, the theory is only briefly introduced in this section. For a more detailed description of the applied RIK (rotational-isotropic-kinematic) hardening model the interested reader is referred to [Choi et al. 2006a].

For the isotropic hardening, we chose a description based on [Chaboche 1989], modified to improve the agreement between experiments and predictions for tensile stress-strain curves [Chun et al. 2002]. The magnitude of the yield stress corresponding to isotropic hardening is described as

$$\bar{\sigma}_y = \bar{\sigma}_0 + K(1 - e^{Ns}) - \frac{c_1}{b_1}(1 - e^{b_1 s}) - c_2 s,$$

where $s$ is the effective plastic strain, $\bar{\sigma}_0$ is the initial yield stress, $K$ and $N$ are fit parameters of the hardening curve in monotonic loading in RD, and $c_1$, $c_2$, $b_1$ are parameters associated with the kinematic hardening and coupling the isotropic to the kinematic hardening.

A related kinematic hardening model with permanent softening, similar to that of [Armstrong and O. 1966], is defined with different backstress terms whose evolution equations are given by

$$\boldsymbol{\alpha}_1^{\nabla} = \frac{c_1}{\beta}(\boldsymbol{\tau} - \boldsymbol{\alpha})\dot{s} - b_1 \dot{s}\boldsymbol{\alpha}_1, \quad \boldsymbol{\alpha}_2^{\nabla} = k\frac{c_2}{\beta}(\boldsymbol{\tau} - \boldsymbol{\alpha})\dot{s}, \tag{2}$$

where $\boldsymbol{\tau}$ denotes the Kirchhoff stress, $\boldsymbol{\alpha} = \boldsymbol{\alpha}_1 + \boldsymbol{\alpha}_2$ is total backstress of the backstress components $\boldsymbol{\alpha}_1, \boldsymbol{\alpha}_2$, and the variable $\beta$ is defined by

$$\beta = \sqrt{\frac{2}{3}} \left\| \frac{\partial \phi}{\partial \boldsymbol{\tau}} \right\|.$$

The Oldroyd rate $(\cdot)^{\nabla}$ is applied for the stress and backstress evolution equations as suggested in [Haupt and Tsakmakis 1986] and [Han et al. 2003].

The rotational hardening is expressed by the rotation of the symmetry axes of anisotropy, $\boldsymbol{e}_i^{\phi}$, defining the orientation of the anisotropic yield function $\phi$. The rotation of the symmetry axes is described by

$$\dot{\boldsymbol{e}}_i^{\phi} = \boldsymbol{\theta}^{\phi} \boldsymbol{e}_i^{\phi},$$

where the constitutive spin $\boldsymbol{\theta}^{\phi}$ is implicitly determined by the material spin $\boldsymbol{w}$ describing rigid body rotations and the plastic spin $\boldsymbol{\omega}_p$, in the following manner:

$$\boldsymbol{\theta}^{\phi} = \boldsymbol{w} - \boldsymbol{\omega}_p^{\phi}.$$

With the introduction of the plastic spin into the model, the anisotropy axes are allowed to rotate relative to the rigid body rotations. Several expressions have been suggested in the literature to describe plastic spin, for example, [Dafalias 1993; 2000; 2001]. Here we consider the expressions suggested in [Han et al. 2002], which describe the experimentally determined rotations of [Kim and Yin 1997] fairly well with

$$\boldsymbol{\omega}_p^{\phi} = \frac{a}{\bar{\sigma}_y} \tan(\vartheta)(\boldsymbol{\tau}\dot{\boldsymbol{\varepsilon}}_p - \dot{\boldsymbol{\varepsilon}}_p\boldsymbol{\tau}), \tag{3}$$

where $a$ is the only material parameter needed to describe the plastic spin. This parameter can be identified with the evolution of $R_{45}$, the $R$-value for specimens at 45° to the RD.

Assuming that the anisotropy axes remain orthogonal during deformation, all these components can be incorporated into the yield function

$$\Phi = \phi - \bar{\sigma}_y^2,$$

where $\phi = (\boldsymbol{\tau} - \boldsymbol{\alpha}) \cdot \boldsymbol{K}_{\phi}(\boldsymbol{\tau} - \boldsymbol{\alpha})$ characterizes a Hill-type yield surface with the fourth order tensor $\boldsymbol{K}_{\phi}$ reflecting the anisotropy and the total backstress is obtained as $\boldsymbol{\alpha} = \boldsymbol{\alpha}_1 + \boldsymbol{\alpha}_2$. For plane stress problems the initial matrix form of the fourth order tensor $\boldsymbol{K}_{\phi}$ can be given in vector notation as

$$\boldsymbol{P}^0 = \begin{bmatrix} 1 & -\beta_{12} & 0 \\ -\beta_{12} & \beta_{22} & 0 \\ 0 & 0 & \beta_{66} \end{bmatrix}, \qquad \boldsymbol{\tau} = \begin{bmatrix} \tau_{11} \\ \tau_{22} \\ \tau_{12} \end{bmatrix}, \qquad \boldsymbol{\alpha} = \begin{bmatrix} \alpha_{11} \\ \alpha_{22} \\ \alpha_{12} \end{bmatrix},$$

where the components are related to $R$-values through

$$\beta_{12} = \frac{R_0}{1 + R_0}, \qquad \beta_{22} = \frac{R_0(1 + R_{90})}{R_{90}(1 + R_0)}, \qquad \beta_{66} = \frac{(R_0 + R_{90})(1 + 2R_{45})}{R_{90}(1 + R_0)};$$

see [Valliappan et al. 1976].

The mechanical tests and texture analysis illustrated in [Boehler and Koss 1991] indicate that the rotation of the anisotropy axes can be related to texture development and rotation of grains. The grain rotation in turn will also affect the backstresses and kinematic hardening as back stresses are usually related to dislocation substructures. The mechanisms of backstresses are however not very well understood. One difficulty may be seen in the different length scales backstresses are associated with; for example, Barton et al. [1999] pointed out that Bauschinger effects can in part be explained by texture development but it is also well known that grain boundaries, dislocation cells [Hughes et al. 2003] and dislocation structures within grains and cells [Feaugas 1999] can have significant influence on the kinematic hardening.

Here the rotation of anisotropy axes is assumed to have an influence on the backstress and an interrelation is suggested here by assuming that the function $k$ in equation (2) depends on the loading directions and anisotropy axes; specifically, $k$ is suggested to have the form

$$k(\varphi, \vartheta) = \begin{cases} 1 + \kappa\vartheta & \text{for initial loading,} \quad \varphi \le \pm 90^\circ, \\ \kappa\vartheta & \text{for reversal loading,} \quad \varphi > \pm 90^\circ, \end{cases} \tag{4}$$

where $\vartheta$ is the angle between the direction of the symmetry axes and direction of straining as shown in Figure 8 and $\varphi$ is the angle between the directions of the previous and current loadings. The angle $\vartheta \in (0, \pi/4)$ is defined by

$$\vartheta = \min\left(\cos^{-1}\frac{\boldsymbol{e}_i^{\phi} \cdot \boldsymbol{n}}{|\boldsymbol{e}_i^{\phi}|\,|\boldsymbol{n}|}\right),$$

where $\boldsymbol{e}_i^{\phi}$ is the direction vector of the anisotropy axes and $\boldsymbol{n}$ is one of the eigenvectors of the strain tensor closer to $\boldsymbol{e}_i^{\phi}$, and angle $\varphi$ is defined by

$$\varphi = \cos^{-1}\frac{\dot{\boldsymbol{\varepsilon}}_p^* \cdot \dot{\boldsymbol{\varepsilon}}_p}{\left|\dot{\boldsymbol{\varepsilon}}_p^*\right|\left|\dot{\boldsymbol{\varepsilon}}_p\right|},$$

where $\dot{\boldsymbol{\varepsilon}}_p^*$ is the plastic strain increment of the previous load step and $\dot{\boldsymbol{\varepsilon}}_p$ is the plastic strain increment of the current loading step. Other approaches where the interaction between kinematic and rotational hardening has been considered are found in [Dafalias 1993; 1998; Tsakmakis 2004].

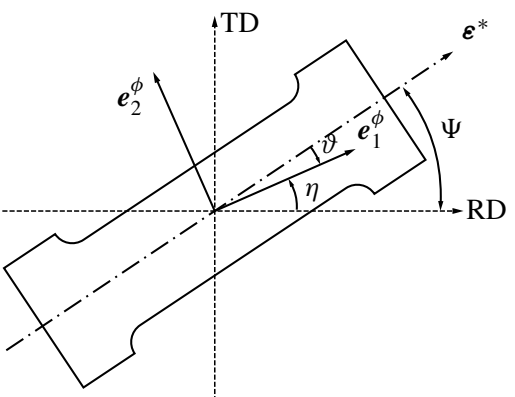


**Figure 8.** Definition of the angles used in formulation: $\Psi$ is the initial orientation to the RD, $\eta$ the rotation angle of the symmetry axes of anisotropy, and $\vartheta = \Psi - \eta$ the difference between the major strain direction and the symmetry axes.

The nonlinear kinematic hardening parameters $c_1$, $b_1$, and $c_2$ in equations (2) are identified by using an inverse method, which optimizes the parameters using the results of three-point bend experiments [Zhao and Lee 1999; 2000]. If rotational hardening is ignored, $a$ and $\kappa$ can be set to zero. Then the RIK hardening model reduces to Chun's ANK model [Chun et al. 2002]. The hardening model reduces to Chaboche's model [1989] if $c_2$ is set to zero, and to a regular isotropic hardening model if $c_1$ and $b_1$ are set to zero. It should be noted that the description of $k$ in Equation (4) could theoretically result in a discontinuous response. In numerical tests however such discontinuities have never occurred — neither in implicit nor explicit finite element simulations [Choi et al. 2006a; 2006b].

## 5. Experimental results and material parameters

The experimental results, the determination of the plastic spin parameters, and the corresponding predictions are discussed in this section. All experimental results presented in this paper are averages over three different tensile tests. The investigated materials are mild steels for deep drawing quality (DDQ) and drawing quality (DQ) and a high strength steel (HSS). The results for DDQ and DQ are shown in Figure 9. The transverse strain values are fit to the longitudinal strain by $\varepsilon_w = \{a \ln(\varepsilon_l) + b\}\varepsilon_l$. The procedure to determine the plastic spin parameters will be described for the DDQ steel material in the following. The determination of the plastic spin parameters involves the results of experiments described in the previous sections or, alternatively, experimental data given in the proceedings of

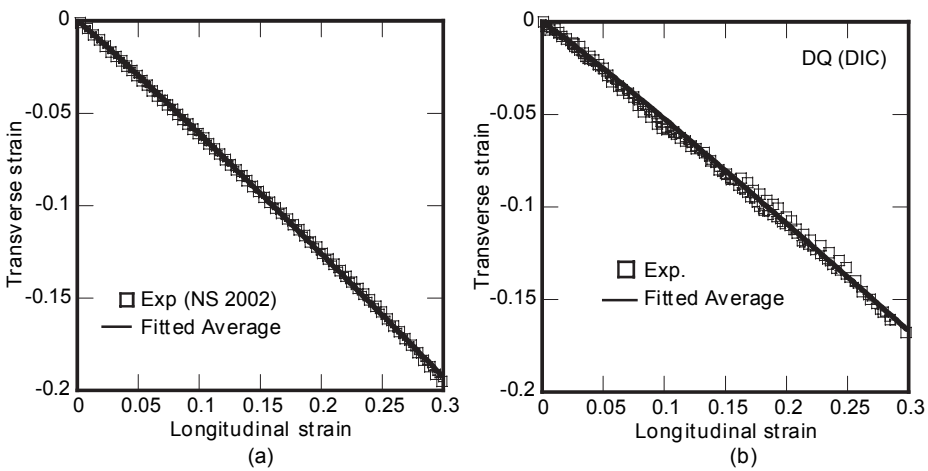


**Figure 9.** Average fitted curves of the transverse and longitudinal strain measurement for 45° orientation tensile tests: (a) DDQ; (b) DQ.

| Material | Elastic | Anisotropy | Isotropic | Kinematic | Rotational |
|---|---|---|---|---|---|
| DDQ (Exp.) | $E = 210\,\text{GPa}$<br>$\nu = 0.3$ | $R_0 = 2.137$<br>$R_{45} = 0.93$<br>$R_{90} = 1.508$ | $\sigma_0 = 152.22\,\text{MPa}$<br>$K = 222.01\,\text{MPa}$<br>$N = -7.87$ | $c_1 = 3.0\,\text{GPa}$<br>$b_1 = 300$<br>$c_2 = 70.0\,\text{MPa}$ | $a = -155$<br>$\kappa = 50.0$ |
| DDQ (NS2002) | $E = 210\,\text{GPa}$<br>$\nu = 0.3$ | $R_0 = 2.722$<br>$R_{45} = 1.474$<br>$R_{90} = 2.169$ | $\sigma_0 = 152.0\,\text{MPa}$<br>$K = 235.81\,\text{MPa}$<br>$N = 9.23$ | $c_1 = 3.0\,\text{GPa}$<br>$b_1 = 300$<br>$c_2 = 70.0\,\text{MPa}$ | $a = -57$<br>$\kappa = 1.8$ |
| DQ | $E = 180\,\text{GPa}$<br>$\nu = 0.3$ | $R_0 = 1.60$<br>$R_{45} = 1.010$<br>$R_{90} = 1.46$ | $\sigma_0 = 198.0\,\text{MPa}$<br>$K = 242.47\,\text{MPa}$<br>$N = 9.95$ | $c_1 = 3.3\,\text{GPa}$<br>$b_1 = 220$<br>$c_2 = 103\,\text{MPa}$ | $a = -100$<br>$\kappa = 1.5$ |
| HSS | $E = 210\,\text{GPa}$<br>$\nu = 0.3$ | $R_0 = 0.832$<br>$R_{45} = 1.185$<br>$R_{90} = 0.560$ | $\sigma_0 = 332.22\,\text{MPa}$<br>$K = 430.55\,\text{MPa}$<br>$N = 1.7$ | $c_1 = 3.0\,\text{GPa}$<br>$b_1 = 150$<br>$c_2 = 80\,\text{MPa}$ | $a = 0$<br>$\kappa = 0$ |

**Table 1.** Material properties of RIK hardening model for DDQ, DQ and HSS.

NUMISHEET 2002. The experimental results for the other materials are shown with fitted curves, and the parameters for all materials are summarized in Table 1.

***DDQ (Experiment with DIC).*** The DDQ sheet metal tested in the experiments is the same material as in the NUMISHEET 2002 benchmark problems [Yang et al. 2002]. The measured transverse strain versus longitudinal strain curves for the RD, TD and 45° to RD direction are shown in Figure 10, together with the corresponding flow curves. Also shown in Figure 10(b) are simulation results of conventional models without rotational hardening. When the rotational evolution of the anisotropy is not considered and $R_{45}$ is fixed at a value measured between 0% and 5% strain, the strain-strain relation for the 45° orientation prediction is higher than the experimental results. The estimated flow curve for the 45° orientation differs from the experimental results after approximately 5% strain. The ratio of stress evolution between 0% and 5% strain correlates well with the experiment. For larger deformations, better results can be obtained when an averaged $R_{45}$ value is applied which is computed from the linear fit of the strain-strain relation from 0% to 20% strain.

Comparisons of experiments and predictions of a conventional hardening model using the averaged $R_{45}$ value are given in Figure 11. Even though the predicted stress level is much closer to the experimental result than the prediction using initial anisotropy values in Figure 10(b), the rate of stress evolution does not correlate with the experimental results for the whole strain range.

With conventional hardening models, the anisotropy of the yield function remains unchanged during the deformation process. Therefore, the evolution of the anisotropy in 45° to the RD cannot be predicted with qualitatively or quantitatively satisfying accuracy. As can be seen in Figure 12(a), this evolution of $R_{45}$ value is present for DDQ material and can be captured with the appropriate rotational hardening parameter. The corresponding flow stresses of tensile tests in the 45° to RD evolve with an abrupt change in stress as the symmetry axes rotate, obeying the

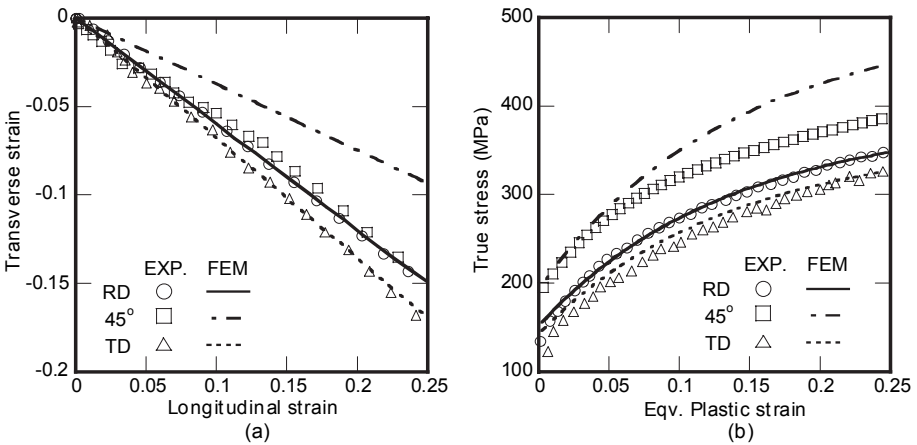


**Figure 10.** Comparing simulation and experimental results of the *initial* $R$-value for 45° orientation: (a) in transverse strain versus longitudinal strain; (b) in the flow stresses.

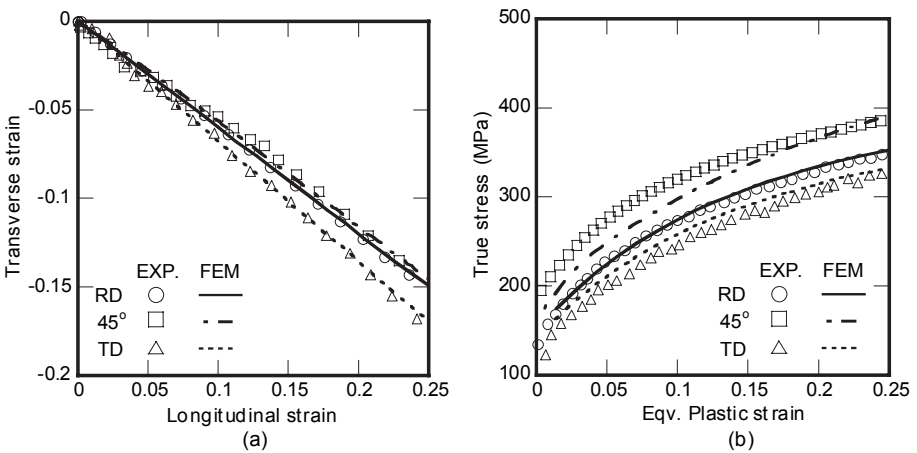


**Figure 11.** Comparing simulation and experimental results of the *averaged* $R$-value for 45° orientation: (a) Transverse strain versus longitudinal strain; (b) flow stresses in each orientation.

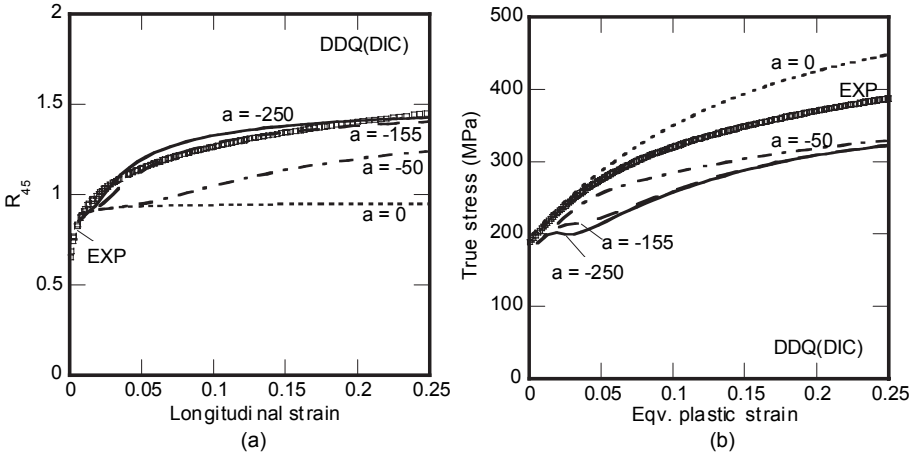


**Figure 12.** Sensitivity of plastic spin parameter: (a) $R_{45}$ evolution; (b) flow stresses of 45° orientation. The softening due to the rotational hardening will be compensated for by backstress.

plastic spin description for the rotation of anisotropy axes. The corresponding flow stress results of experiments and predictions with various values for the parameter $a$ are shown in Figure 12(b).

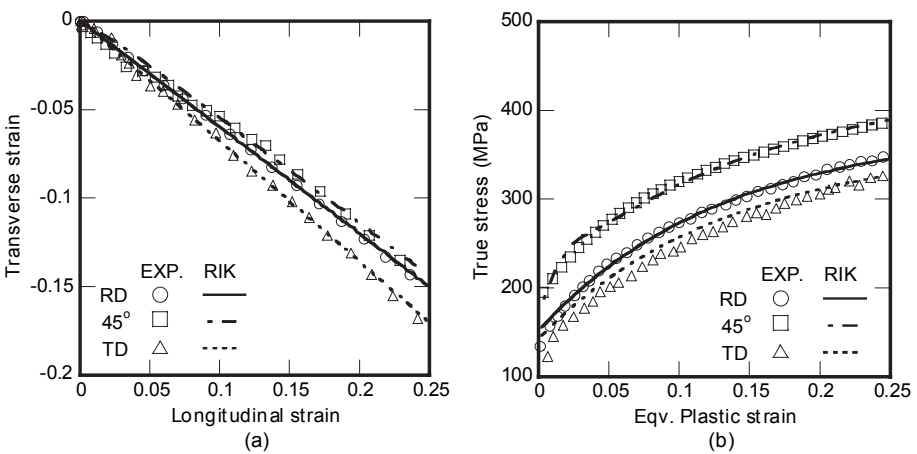


**Figure 13.** Simulation with the RIK hardening model and comparison with experimental results: (a) transverse strain versus longitudinal strain, (b) flow stresses in each orientation. For the 45° orientation the flow stress loss due to the rotational hardening is recovered by the backstress.

The diagrams related to stretch tests in RD and TD are omitted because there is no rotation in these two directions and the predictions in these directions are identical to those without rotational hardening. A plastic spin parameter of $a = -155$ is found to be the best fit for the experimental $R_{45}$ data in Figure 12(a). The differences between experimental and computed flow stress curves in Figure 12(b) are then corrected by adding kinematic hardening through equation (4). As shown in Figure 13, kinematic hardening improves the fit to the experimental flow stress curves without changing the slope of the strain-strain curves.

***DDQ (NUMISHEET 2002 Data).*** Figure 1 showed the flow stress versus strain curves of the DDQ material from NUMISHEET 2002, and Figure 2 the transverse strain versus longitudinal strain curves. As discussed on page 304, conventional

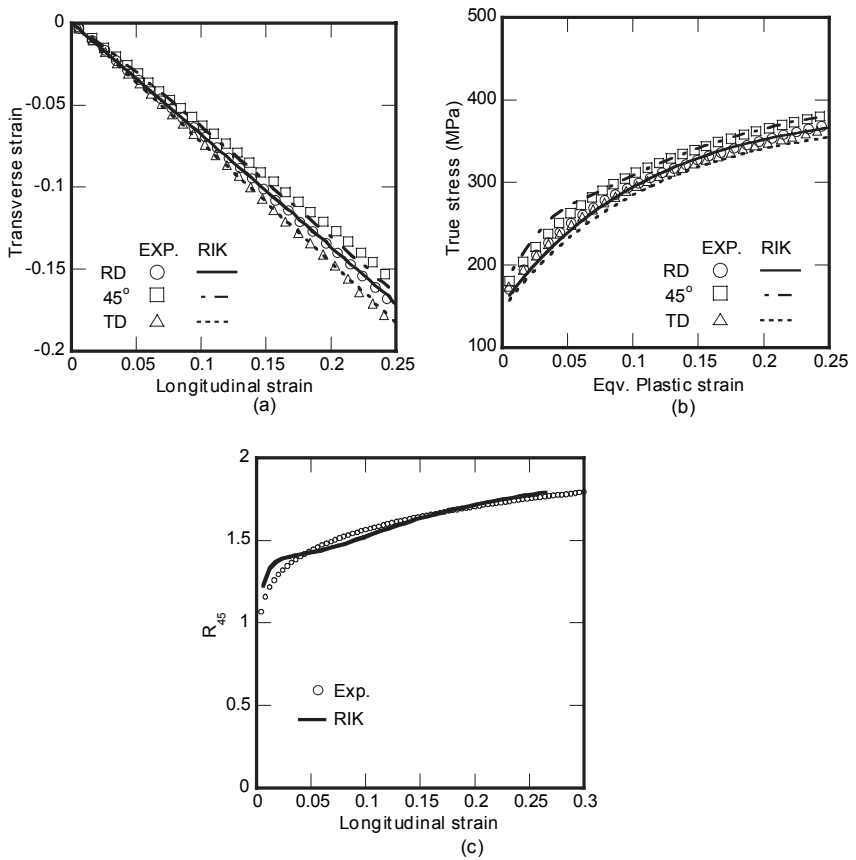


**Figure 14.** Results for DDQ mild steel using data from NUMISHEET 2002: (a) transverse strain versus longitudinal strain; (b) flow stress curves in each orientation; (c) $R_{45}$ evolution.

models without rotational hardening overestimate the flow stress by applying the average $R$-value for the 45° orientation stretch tests.

Figure 14 plots the predictions obtained with the RIK hardening model together with the experimental results. Parts (a) and (b) show there is good agreement in the case of transverse strain versus longitudinal strain and stress versus strain. By applying a plastic spin parameter, $a = -155$, the change of $R_{45}$ is reasonably well represented, as shown in Figure 14(c).

***DQ mild steel.*** In addition to DDQ mild steel, drawing quality (DQ) mild steel was also examined. The same procedure applied to DDQ mild steel was performed for DQ mild steel. The strain-strain, strain-stress at 45° to RD and strain-$R_{45}$ results

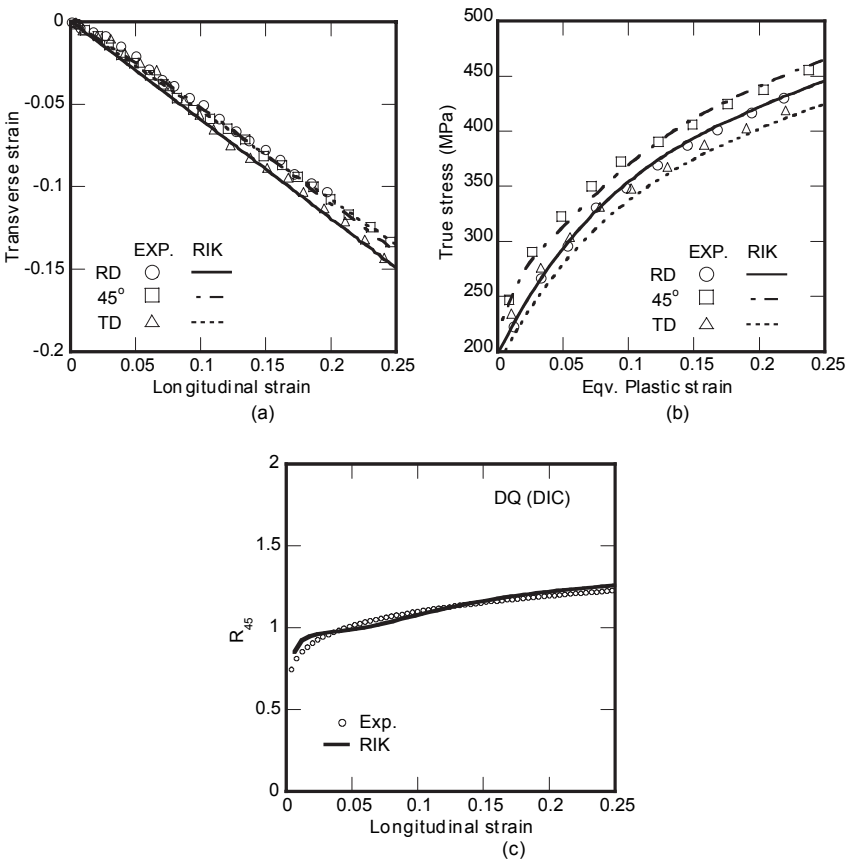


**Figure 15.** Results for DQ mild steel: (a) Transverse strain versus longitudinal strain; (b) Flow stresses of the RD, 45° and the TD; (c) $R_{45}$ evolution.

from experiments and simulations are illustrated in Figure 15. Experiments and predictions show excellent agreement for a wide range of applied strains.

***HSS.*** High strength steel (HSS) is a material widely used in the automotive industry and, like the mild steels discussed above, it is subject to large strain in the forming processes. This material was also tested for rotational hardening. In contrast to the mild steels described earlier, HSS does not show much rotation, since its $R_{45}$-values do not significantly change during deformation. Consequently, the spin parameter is set to zero for this material, which corresponds to anisotropy axes aligned with the material axes. Experimental and computational results are compared in Figure 16.

## 6. Discussion

By comparing the $R$-values of the different materials, it can be concluded that only the HSS material has a $R_{45}$-value higher than the $R$-values in RD and TD. Thus, the HSS material in the 45° orientation does not exhibit rotation of the anisotropy axes toward the straining direction as in the DDQ and DQ materials. Furthermore, for HSS, the flow curves are actually modeled with good agreement by applying initial $R$-values determined from the transverse strain versus longitudinal strain curves. Therefore, it may be assumed that the rotational hardening in HSS is very small. For these tests, the anisotropy of HSS hardly evolves with the deformation. This may be due to a pronounced texture that is not severely affected by the deformation of the tensile tests. To verify this interpretation, we recall the results of Boehler and Koss [1991] and Bunge and Nielsen [1997] who determined symmetry axes

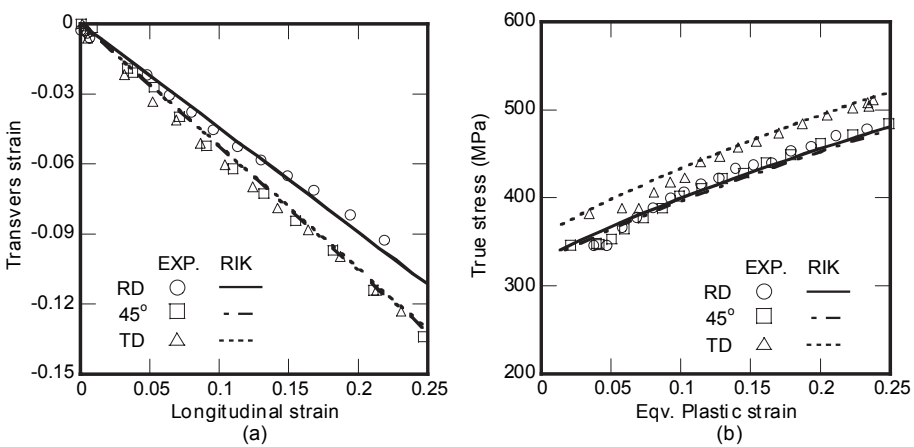


**Figure 16.** Results for HSS: (a) transverse strain versus longitudinal strain; (b) flow stresses of the RD, 45°, and the TD.

by texture analysis via orientation distribution function (ODF). In the first of these references, significant rotations of the symmetry axes for mild steel were observed in pole figures, whereas in the second, the rotation of the symmetry axes is quite small for cold rolled aluminum, where the texture is quite pronounced. The same may be true for HSS; this would have to be confirmed by monitoring the texture.

The $R$-values are used to compare the anisotropy of materials in a quantitative manner. The $R$-values measured in tensile experiments are useful for predicting the rotational evolution of anisotropy. On the other hand, $\bar{R}$ and $\Delta R$, which are defined as

$$\bar{R} = \frac{R_0 + 2R_{45} + R_{90}}{4}, \quad \Delta R = \frac{R_0 - 2R_{45} + R_{90}}{2},$$

are also used to judge the formability ($\bar{R}$) and the earing pattern ($\Delta R$) in applied problems like the circular cup drawing. Formability increases as $\bar{R}$ increases. For mild steel with rotational hardening, $\bar{R}$ changes with respect to $R_{45}$ during deformation, in agreement with experimental results. Therefore, it may be concluded that models with rotational hardening can describe the formability better than non-rotational hardening models.

The plastic spin in sheet metals implicitly defines the planar rotation of the symmetry axes of anisotropy, and $\Delta R$ is known to be related to the planar anisotropy. Therefore, there must be a relationship between the parameters of the plastic spin and the planar anisotropy $\Delta R$. The plastic spin and planar anisotropy values for the tested materials are shown in Table 1. As shown in Figure 17, there is evidence that the plastic spin may be linearly related to $\Delta R$. Detailed experimental determination of the rotation of the symmetry axes of anisotropy would help to verify these results. In Figure 17 the comparison between the plastic spin parameter

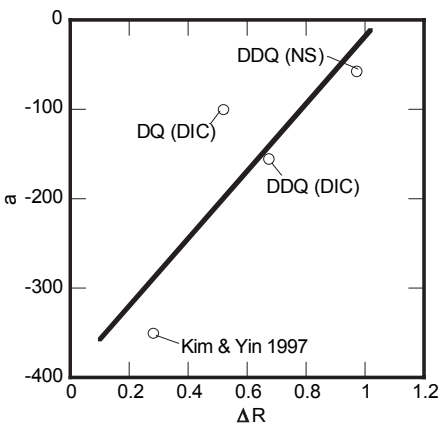


**Figure 17.** Plastic spin parameter $a$ versus planar anisotropy $\Delta R$.

using the measured data of the rotation of the symmetry axes [Kim and Yin 1997] shows good correlation. Therefore, it may be possible to determine the unknown plastic spin parameter from the $R$-values ($\Delta R$) for mild steel. More experiments are required to verify this methodology for other alloys and crystal structures.

## 7. Concluding remarks

For two mild steels and a high strength steel sheet metal, experimental results of conventional flow stress curves and transverse versus longitudinal strain curves of two orientations relative to the RD have been presented. Assuming that rotation of the anisotropy axes can describe the evolution of anisotropy qualitatively, the material parameters for the plastic spin and for correcting the kinematic hardening description can be identified from tensile tests. Using the DIC method, it is relatively easy to measure large strains. The DIC method was applied to generate experimental transverse strain versus longitudinal strain for simple tensile tests. The evolution of anisotropy is then correlated with the slope of the transverse strain versus longitudinal strain curve. Only the plastic spin parameter allows a change to the slope of the computed transverse strain versus longitudinal strain curve. The flow stress results can further be improved by incorporating the kinematic hardening. The parameters for the RIK model can be determined by three-point bend tests [Zhao and Lee 1999; 2001] and tensile tests for three directions: RD, TD, and 45°. With the aid of the rotational evolution of the anisotropy axes, the RIK model can essentially capture anisotropic plastic hardening behavior with Hill's quadratic yield criteria. For mild steel, a linear relationship between the planar anisotropy $\Delta R$ and the plastic spin parameter $a$ has been determined.

## Acknowledgment

The contributions of Hyungjun Kim in the setup and execution of the uniaxial experiments using DIC is highly appreciated.

## References

[Agnew and Weertman 1998] S. R. Agnew and J. R. Weertman, "The influence of texture on the elastic properties of ultrafine-grain copper", *Mater. Sci. Eng. A* **242**:1 (1998), 174–180.

[Armstrong and O. 1966] P. J. Armstrong and F. C. O., "A mathematical representation of the multiaxial Bauschinger effect", Report rd/b/bn 731, Central Electricity Generating Board, 1966.

[Asaro 1983] R. J. Asaro, "Micromechanics of crystals and polycrystals", *Adv. Appl. Mech.* **23** (1983), 1–115.

[Banabic et al. 2000] D. Banabic, H. J. Bunge, K. Pohlandt, and A. E. Tekkaya, *Formability of metallic materials*, Springer, 2000.

[Barlat et al. 1991] F. Barlat, D. J. Lege, and J. C. Brem, "A six-component yield function for anisotropic materials", *Int. J. Plast.* **7**:7 (1991), 693–712.

[Barlat et al. 1997] F. Barlat, Y. Maedat, K. Chung, M. Yanagawa, J. C. Brem, Y. Hayashida, D. J. Lege, K. Matsui, S. J. Murtha, S. Hattori, R. C. Becker, and S. Makosey, "Yield function development for aluminum alloy sheets", *J. Mech. Phys. Solids* **45**:11 (1997), 1727–1763.

[Barlat et al. 2003] F. Barlat, J. C. Brem, J. W. Yoon, K. Chung, R. E. Dick, D. J. Lege, F. Pourboghrat, S. H. Choi, and E. Chu, "Plane stress yield function for aluminum alloy sheets, I: theory", *Int. J. Plast.* **19**:9 (2003), 1297–1319.

[Barton et al. 1999] N. Barton, P. R. Dawson, and M. Miller, "Yield strength asymmetry predictions from polycrystal elastoplasticity", *J. Eng. Mater. Technol.* ( *ASME* ) **121**:2 (1999), 230–239.

[Beaudoin et al. 1994] A. J. Beaudoin, P. R. Dawson, K. K. Mathur, U. F. Kocks, and D. A. Korzekwa, "Application of polycrystal plasticity to sheet forming", *Comput. Methods Appl. Mech. Eng.* **117**:1–2 (1994), 49–70.

[Boehler and Koss 1991] J. P. Boehler and S. Koss, "Evolution of anisotropy in sheet-steels submitted to off-axes large deformations", pp. 143–158 in *Advances in continuum mechanics*, edited by O. e. a. Brueller, Springer, 1991.

[Bunge and Nielsen 1997] H. J. Bunge and I. Nielsen, "Experimental determination of plastic spin in polycrystalline materials", *Int. J. Plast.* **13**:5 (1997), 435–446.

[Chaboche 1989] J. L. Chaboche, "Constitutive equations for cyclic plasticity and cyclic viscoplasticity", *Int. J. Plast.* **5**:3 (1989), 247–302.

[Choi et al. 2006a] Y. Choi, C. S. Han, J. K. Lee, and R. H. Wagoner, "Modeling multi-axial elastoplastic deformation of planar anisotropic materials, I: Theory", *Int. J. Plast.* **22**:9 (2006), 1745–1764.

[Choi et al. 2006b] Y. Choi, C. S. Han, J. K. Lee, and R. H. Wagoner, "Modeling multi-axial elastoplastic deformation of planar anisotropic materials, II: Applications", *Int. J. Plast.* **22**:9 (2006), 1765–1783.

[Chun et al. 2002] B. K. Chun, J. T. Jinn, and J. K. Lee, "Modeling of the Bauschinger effect for sheet metals, I: Theory", *Int. J. Plast.* **18**:5 (2002), 571–595.

[Dafalias 1993] Y. F. Dafalias, "On multiple spins and texture development, Case study: kinematic and orthotropic hardening", *Acta Mech.* **100**:3–4 (1993), 171–194.

[Dafalias 1998] Y. F. Dafalias, "Plastic spin: Necessity or redundancy?", *Int. J. Plast.* **14**:9 (1998), 909–931.

[Dafalias 2000] Y. F. Dafalias, "Orientational evolution of plastic orthotropy in sheet metals", *J. Mech. Phys. Solids* **48**:11 (2000), 2231–2255.

[Dafalias 2001] Y. F. Dafalias, "Plasticity in large deformations", pp. 247–254 (Section 4.8) in *Handbook of materials behavior models*, edited by J. Lemaitre, Academic Press, 2001.

[Feaugas 1999] X. Feaugas, "On the origin of the tensile flow stress in the stainless steel AISI 316L at 300 K: back stress and effective stress", *Acta Mater.* **47**:13 (1999), 3617–3632.

[Han et al. 2002] C. S. Han, Y. Choi, J. K. Lee, and R. H. Wagoner, "A FE formulation for elastoplastic materials with planar anisotropic yield functions and plastic spin", *Int. J. Solids Struct.* **39**:20 (2002), 5123–5141.

[Han et al. 2003] C. S. Han, M. G. Lee, K. Chung, and R. H. Wagoner, "Integration algorithms for planar anisotropic shells with isotropic and kinematic hardening at finite strains", *Commun. Numer. Methods Eng.* **19**:6 (2003), 473–490.

[Haupt and Tsakmakis 1986] P. Haupt and C. Tsakmakis, "On kinematic hardening and large plastic deformation", *Int. J. Plast.* **2**:3 (1986), 279–293.

[Hill 1948] R. Hill, "A theory of the yielding and plastic flow of anisotropic metals", *P. Roy. Soc. Lond. A Mat.* **193**:1033 (1948), 281–297.

[Hill 1950] R. Hill, *The mathematical theory of plasticity*, Oxford University Press, 1950.

[Hill 1990] R. Hill, "Constitutive modeling of orthotropic plasticity in sheet metals", *J. Mech. Phys. Solids* **38**:3 (1990), 405–417.

[Hughes et al. 2003] D. A. Hughes, N. Hansen, and D. J. Bammann, "Geometrically necessary boundaries, incidental dislocation boundaries and geometrically necessary dislocations", *Scr. Mater.* **48**:2 (2003), 147–153.

[Kim and Yin 1997] K. H. Kim and J. J. Yin, "Evolution of anisotropy under plane stress", *J. Mech. Phys. Solids* **45**:5 (1997), 841–851.

[Kocks et al. 1998] U. F. Kocks, C. N. Tome, and H. R. Wenk, *Texture and anisotropy*, Cambridge University Press, 1998.

[Kuroda 1997] M. Kuroda, "Interpretation of the behavior of metals under large plastic shear deformations: a macroscopic approach", *Int. J. Plast.* **13**:4 (1997), 359–383.

[Nakamachi and Doug 1997] E. Nakamachi and X. Doug, "Study of texture effect on sheet failure in a limit dome height test by using elastic/crystalline viscoplastic finite element analysis", *J. Appl. Mech.* (*ASME*) **64**:3 (1997), 519–524.

[Peeters et al. 2001] B. Peeters, M. Seefeldt, C. Tedodosiu, S. R. Kalidindi, P. Van Houtte, and E. Aernoudt, "Work-hardening/softening behavior of B.C.C. polycrystals during changing strain paths: I. An integrated model based on substructure and texture evolution, and its prediction of the stress-strain behavior of an IF steel during two-stage strain paths", *Acta Mater.* **49**:9 (2001), 1607–1629.

[Rao and Mohan 2001] K. P. Rao and E. V. R. Mohan, "A vision-integrated tension test for use in sheet-metal formability studies", *J. Mater. Process. Technol.* **118**:1–3 (2001), 238–245.

[Sutton et al. 1983] M. A. Sutton, W. J. Wolters, W. H. Peters, W. F. Ranson, and S. R. McNeill, "Determination of displacements using an improved digital correlation method", *Image Vision Comput.* **1**:3 (1983), 133–139.

[Tsakmakis 2004] C. Tsakmakis, "Description of plastic anisotropy effects at large deformations, I: restrictions imposed by the second law and the postulate of Il'iushin", *Int. J. Plast.* **20**:2 (2004), 167–198.

[Valliappan et al. 1976] S. Valliappan, P. Boonlaulohr, and I. K. Lee, "Non-linear analysis for anisotropic materials", *Int. J. Numer. Meth. Eng.* **10**:3 (1976), 597–606.

[Vendroux and Knauss 1998] G. Vendroux and W. G. Knauss, "Submicron deformation field measurements, 2: Improved digital image correlation", *Exp. Mech.* **38**:2 (1998), 86–92.

[Yang et al. 2002] D. Y. Yang, S. I. Oh, H. Huh, and Y. H. Kim, "NUMISHEET 2002", Proceedings -Verification of Simulations with Experiments, 2002.

[Zhao and Lee 1999] K. Zhao and J. K. Lee, "On simulation of bending/reverse bending of sheet metals", *J. Manuf. Sci. Eng.* (*ASME*) **10** (1999), 929–933.

[Zhao and Lee 2000] K. Zhao and J. K. Lee, "Generation of cyclic stress-strain curves for sheet metals", *ASME MED* **11** (2000), 667–674.

[Zhao and Lee 2001] K. Zhao and J. K. Lee, "Generation of cyclic stress-strain curves for sheet metals", *J. Eng. Mater. Technol.* (*ASME*) **123**:4 (2001), 391–397.

Received 22 Oct 2005. Revised 27 Nov 2005.

YANGWOOK CHOI: yangwook.choi@abaqus.com

*Dr. Yangwook Choi, Department of Mechanical Engineering, The Ohio State University, 650 Ackerman Road, Columbus, Ohio 43210, United States*

MARK E. WALTER: walter.80@osu.edu
*Dr. Mark E. Walter, Department of Mechanical Engineering, The Ohio State University, 650 Ackerman Road, Columbus, Ohio 43210, United States*

JUNE K. LEE: lee.71@osu.edu
*Dr. June K. Lee, Department of Mechanical Engineering, The Ohio State University, 650 Ackerman Road, Columbus, Ohio 43210, United States*

CHUNG-SOUK HAN: chung-souk.han@ndsu.edu
*Dr. Chung-Souk Han, Department of Civil Engineering, North Dakota State University, 1410 North 14th Avenue, Fargo, ND 58105, United States*